ARTICLE IN PRESS

Available online at www.sciencedirect.com
SCIENCE DIRECT®

Physica D xxx (2004) xxx–xxx

PHYSICA D

www.elsevier.com/locate/physd

Nonextensive statistical mechanics for rotating quasi-two-dimensional turbulence

Sunghwan Jung, Brian D. Storey, Julien Aubert, Harry L. Swinney*

Department of Physics, Center for Nonlinear Dynamics, The University of Texas at Austin, Austin, TX 78712, USA

Communicated by C.K.R.T. Jones

Abstract

We have conducted experiments on an asymmetrically forced quasi-two-dimensional turbulent flow in a rapidly rotating annulus. Assuming conservation of potential enstrophy and energy, we maximize a nonextensive entropy function to obtain the azimuthally averaged vorticity as a function of radial position. The predicted vorticity profile is in good accord with the observations. A nonextensive formalism is appropriate because long-range correlations between small-scale vortices give rise to large coherent structures in the turbulence. We also derive probability distribution functions for the vorticity from both extensive and nonextensive entropies, and we find that the prediction from nonextensive theory is in better accord with experiment, especially in the tails of the distribution function. The nonextensive parameter q has the value 1.9 ± 0.2.

Keywords: Turbulence; Rotating flows; Tsallis entropy; Nonextensive

1. Introduction

Equilibrium statistical mechanics has long been used to describe turbulence [1]. Early work by Onsager predicted coherent structure formation through consideration of the interactions of point vortices [2]. Later Kraichnan constructed a statistical theory based on energy and enstrophy conservation [3] and showed that the Euler equation (for inviscid flow) with truncation below a certain small length scale could describe turbulent flows [4,5]. More recently, Miller showed that large scale coherent structures could be described by equilibrium statistical mechanics of the Euler equation through a continuous distribution of microscopic vorticity [6]. These analyses assumed that the asymptotic behavior depends upon the values of the conserved quantities rather than on the details of initial structures. Further, the analyses were based on Boltzmann–Gibbs statistics, which only describes weak interactions and does not capture long-range interactions [7]. Our observations of large coherent vortices in experiments on flow in a rotating annulus [8–10] lead us to consider a generalization of statistical mechanics that is applicable to systems with long-range interactions: the nonextensive formalism proposed by Tsallis [11,12].

Probability distribution functions (PDFs) for the velocity increment, $\delta v(r) = \langle v(x+r) - v(x) \rangle_x$, have been derived from nonextensive theory assuming conservation of an *effective energy* proportional to $(\delta v)^2$, and these PDFs have

* Corresponding author. Fax: +1-512-471-1558.
E-mail addresses: sunnyjsh@chaos.utexas.edu (S. Jung), swinney@chaos.utexas.edu (H.L. Swinney).

0167-2789/$ – see front matter © 2004 Published by Elsevier B.V.
doi:10.1016/j.physd.2004.01.035

been found to describe several turbulent flows [13–16]; however, $(\delta v)^2$ is not a conserved quantity for the rotating flows of interest here. Experiments on a plasma of electrons in a strong magnetic field have been interpreted using both extensive entropy [17] and nonextensive entropy [18] with conservation of energy. These analyses did not consider Miller's distinction between the macroscopic and microscopic quantities.

For our laboratory flow, we exploit an additional conservation property that holds for geostrophic flows. A geostrophic flow is one that is dissipationless and rotates sufficiently fast so that it is two-dimensional, varying only in the plane perpendicular to the rotation axis [19]. The additional conserved quantity is the *potential enstrophy*, which is defined as [19,20]

$$\Pi = \int \left(\frac{\omega(\vec{r}) + 2\Omega}{h(r)} \right)^2 \mathrm{d}\vec{r}, \tag{1}$$

where $\omega(\vec{r})$ is the local vorticity and in our system, Ω the rotation rate of the annulus, and h the height of fluid, which increases in the r-direction. A sloping bottom in our rotating annulus models the variation of the Coriolis force with latitude in a real geophysical flow. Flow in our laboratory system is only approximately geostrophic because the rotation rate is finite rather than infinite and the dissipation is nonzero. However, the rotation rate is large enough and dissipation effects are small enough so that the flow is strongly two-dimensional (*quasi-geostrophic*) [9] and the potential enstrophy should be nearly conserved. The potential enstrophy is only one of an infinite number of conserved quantities in a geostrophic flow, $\int \mathrm{d}\vec{r} Q^n$ (with n an integer), where $Q \equiv (\omega + 2\Omega)/h$ is the potential vorticity; the potential enstrophy corresponds to $n = 2$. The higher order conserved terms are more dependent on viscous effects than energy and potential enstrophy terms [21], so we limit our analysis to the two latter conserved quantities, which are often called *rugged invariants* [22–25].

In this paper we use the Euler equation, which neglects viscous dissipation, to obtain predictions of statistical properties of turbulence that we then compare with our experimental observations. The Euler equation has been found to describe phenomena in large scale oceanic and atmospheric flows [6,29,30], and should provide a useful description to flow in our rotating annulus, where dissipation is small, i.e., the spin down time ($=\sqrt{h^2/4\nu\Omega} \approx 25$ s) is much longer than the typical vortex turnover time ($\approx$2 s).

The paper is organized as follows. In Section 2 we briefly describe the nonextensive formalism. In Section 3 we introduce our nonextensive model for two-dimensional flows with energy and enstrophy conservation. We derive expressions for the radial dependence of the azimuthally averaged vorticity and for the probability distribution function of the vorticity; details of these calculations are given in Appendices A and B. In Section 4 we discuss the experiment. In Section 5 we compare the predictions of our model with the experimental data. Finally, in Section 6 we compare the nonextensive parameter q deduced from our work with values obtained in other work.

2. Nonextensive entropy

A system composed of sub-systems A and B has entropy [26]

$$S_q(A + B) = S_q(A) + S_q(B) + (1 - q)S_q(A)S_q(B), \tag{2}$$

where $S_q(A)$ is the entropy of system A and q the nonextensive parameter. When $q = 1$, the entropy is extensive. Tsallis proposed a form of the entropy that satisfies the above equation [12],

$$S_q = \frac{k}{q-1} \left(1 - \sum_i^W p_i^q \right), \tag{3}$$

where W is the total number of possible microstates of the system, p_i the probability of ith state and k the Boltzmann constant. There are two constraints on the system, the normalization

$$\sum_{i=1}^{W} p_i = 1, \tag{4}$$

and the conservation of total energy

$$\frac{\sum_{i=1}^{W} p_i^q E_i}{\sum_{i=1}^{W} p_i^q} = \hat{U}_q, \tag{5}$$

where E_i is the energy of ith state and $\hat{U}_q$ is a normalized q-expectation total energy. The normalized q-expectation of any observable, O, can be expressed as

$$\hat{O}_q = \frac{\sum_{i=1}^{W} p_i^q O_i}{\sum_{i=1}^{W} p_i^q}. \tag{5}$$

Other definitions of observable quantities are inconsistent with the first law of thermodynamics [27].

When a system is in contact with a thermal reservoir, the entropy under appropriate constraints is maximized. The probability p_i of microstate i can be obtained by introducing Lagrange parameters α' and β' and finding the maximum with respect to p_i of

$$\phi_q[p_i] = \frac{S_q}{k} + \alpha' \sum_{i=1}^{W} p_i - \beta' \frac{\sum_{i=1}^{W} p_i^q (E_i - \hat{U})}{\sum_{i=1}^{W} p_i^q}. \tag{7}$$

Solving for p_i yields

$$p_i = \frac{1}{Z}[1 - (1-q)\beta E_i]^{1/(1-q)}, \tag{8}$$

where $\beta = \beta'/(\sum_j p_j^q + (1-q)\beta'\hat{U})$ and Z is the normalization factor. In the limit $q \to 1$, Boltzmann–Gibbs statistics is recovered, $p_i = (1/Z)\,\mathrm{e}^{-\beta E_i}$.

3. Energy–enstrophy models

We now compute the azimuthally averaged vorticity as a function of radius for the extensive and nonextensive cases and derive expressions for the vorticity probability distribution function. We assume in each case three constraints: normalization, conserved energy, and conserved enstrophy. We follow Miller [6,28] in considering the "microscopic vorticity" field σ, which he used to develop a statistical mechanics formalism for two-dimensional turbulent flows. The macroscopic variables are then defined by averaging the microscopic vorticity, which obeys the conservation laws [28]. The microscopic vorticity is replaced by the probability density function $p(\sigma, \vec{r})$, which is a conserved quantity as a consequence of the incompressibility of the flow [29]. The macroscopic vorticity ω and macroscopic enstrophy ω^2 are defined in terms of the microscopic vorticity σ as

$$\omega(\vec{r}) = \int \mathrm{d}\sigma\, \sigma p(\sigma, \vec{r}), \qquad \omega^2(\vec{r}) = \int \mathrm{d}\sigma\, \sigma^2 p(\sigma, \vec{r}). \tag{9}$$

In the following subsections, we show that the extensive and nonextensive models predict the same radial profile for the vorticity, but predict different vorticity PDFs.

3.1. Extensive model

The conserved energy and potential enstrophy expressed in terms of the microscopic vorticity $p(\sigma, \vec{r})$ are

$$\hat{U} = \int \mathrm{d}\vec{r} \int \mathrm{d}\sigma\, \sigma p(\sigma, \vec{r}) \psi(\vec{r}), \tag{10}$$

$$\hat{\Pi} \approx \int \mathrm{d}\vec{r} |\omega(\vec{r}) + \beta_{\mathrm{Rossby}} r|^2 = \int \mathrm{d}\vec{r} \left(\int \mathrm{d}\sigma (\sigma^2 + 2\beta_{\mathrm{Rossby}} r\sigma) p(\sigma, \vec{r}) + \beta_{\mathrm{Rossby}}^2 r^2 \right), \tag{11}$$

where $\beta_{\mathrm{Rossby}} \equiv 2\eta\Omega/h_0$ is the β-plane coefficient, Ω the rotation rate of the laboratory annulus system, η the slope of the annulus bottom (the β plane), and h_0 the mean depth of the annulus. Eq. (11) follows from Eq. (1) by rescaling for quasi-geostrophic flow [20]. We analyze this rescaled form for the enstrophy.

When the extensive entropy ($S \equiv -kp_i \ln p_i$) is maximized with energy and potential enstrophy constraints using the corresponding Lagrange multipliers β and γ, the probability of the equilibrium state becomes

$$p(\sigma, \vec{r}) = \frac{1}{Z} \mathrm{e}^{-\gamma(\sigma + \beta_{\mathrm{Rossby}} r + (\beta/\gamma)\psi(\vec{r}))^2}, \tag{12}$$

where γ is the Lagrange multiplier of the potential enstrophy.

The radial dependence of the vorticity is obtained from the equation for the stream function, which is derived in Appendix A.1,

$$\nabla^2 \psi - \left(\beta_{\mathrm{Rossby}} r + \frac{\beta}{\gamma} \psi \right) = 0. \tag{13}$$

Solving this equation with appropriate boundary conditions allows us to determine the parameter β/γ by comparing the predicted radial profile of vorticity with our measurements. The results are presented in Section 5.3. The linear relation between our stream function and its Laplacian is similar to a result that was obtained from a minimum enstrophy principle, $\nabla^2\psi + \mu + \lambda\psi = 0$ [31,32].

The PDF of the microscopic vorticity σ can be expressed as

$$g(\sigma) = \int p(\sigma, \vec{r})\, \mathrm{d}\vec{r} = \frac{1}{Z} \int \mathrm{d}\vec{r}\, \mathrm{e}^{-\gamma(\sigma + \beta_{\mathrm{Rossby}} r + (\beta/\gamma)\psi(\vec{r}))^2}. \tag{14}$$

Since the microscopic vorticity σ cannot be measured, this PDF cannot be verified. Miller uses $g(\sigma)$ to compute the PDF of the measurable ("dressed") vorticity in a finite volume [29]. We conduct a similar analysis in Appendix A.2 and obtain the following prediction for the measurable vorticity:

$$g_{\mathrm{d}}(\omega) \propto \int \mathrm{d}\vec{r} \frac{1}{\omega + \beta_{\mathrm{Rossby}} r + (\beta/\gamma)\psi(\vec{r})} \mathrm{e}^{-\gamma(\omega + \beta_{\mathrm{Rossby}} r + (\beta/\gamma)\psi(\vec{r}))^2} \sinh\left(2\gamma\omega_{\mathrm{m}} \left(\omega + \beta_{\mathrm{Rossby}} r + \frac{\beta}{\gamma} \psi(\vec{r}) \right) \right), \tag{15}$$

where ω_{m} is the fluctuation limit of the microscopic vorticity and γ the Lagrange multiplier of the potential enstrophy.

3.2. Nonextensive model

Nonadditivity can be achieved by defining any observable as in Eq. (5). The vorticity and vorticity squared can be redefined within the nonextensive formalism as

$$\omega_q(\vec{r}) = \frac{\int \mathrm{d}\sigma\, \sigma p^q(\sigma, \vec{r})}{\int \mathrm{d}\sigma\, p^q}, \tag{16}$$

$$\omega_q^2(\vec{r}) = \frac{\int \mathrm{d}\sigma\, \sigma^2 p^q(\sigma,\vec{r})}{\int \mathrm{d}\sigma\, p^q}. \tag{17}$$

In the nonextensive formalism, the two conserved quantities, energy and potential enstrophy, become

$$\hat{U} = \frac{\int \mathrm{d}\vec{r} \int \mathrm{d}\sigma\, \sigma p^q(\sigma,\vec{r})\psi(\vec{r})}{\int \mathrm{d}\vec{r} \int \mathrm{d}\sigma\, p^q(\sigma,\vec{r})}, \tag{18}$$

$$\hat{\Pi} \approx \frac{\int \mathrm{d}\vec{r}(\omega+\beta_{\mathrm{Rossby}} r)^2}{\int \mathrm{d}\vec{r} \int \mathrm{d}\sigma\, p^q(\sigma,\vec{r})} = \frac{\int \mathrm{d}\vec{r}\{\int \mathrm{d}\sigma(\sigma^2 + 2\beta_{\mathrm{Rossby}} r\sigma) p^q(\sigma,\vec{r}) + \beta_{\mathrm{Rossby}}^2 r^2\}}{\int \mathrm{d}\vec{r} \int \mathrm{d}\sigma\, p^q(\sigma,\vec{r})}. \tag{19}$$

The PDF for the microscopic entropy, subject to the three constraints (normalization, conserved energy, and conserved enstrophy), becomes

$$p(\sigma,\vec{r}) = \frac{1}{Z}\left[1 - \frac{(1-q)\gamma}{f(\omega)}\left(\sigma + \frac{\beta\psi(\vec{r})}{\gamma} + \beta_{\mathrm{Rossby}} r\right)^2\right]^{1/(1-q)}, \tag{20}$$

where $f(\omega) \equiv 1 + (1-q)\gamma\omega^2$. The expression for the stream function remains identical to the extensive case, Eq. (13). In Appendix B.2 we derive the following PDF of the microscopic vorticity for $q > 1$,

$$\begin{aligned} g(\sigma) &= \int \mathrm{d}\vec{r} \frac{p^q}{\int p^q \mathrm{d}\sigma} \\ &= \Xi \int \mathrm{d}\vec{r}\left[1 - \frac{(1-q)\gamma}{f(\beta_{\mathrm{Rossby}} r + (\beta/\gamma)\psi)}\left(\sigma + \beta_{\mathrm{Rossby}} r + \frac{\beta}{\gamma}\psi\right)^2\right]^{q/(1-q)} f\left(\beta_{\mathrm{Rossby}} r + \frac{\beta}{\gamma}\psi\right)^{-1/2}, \end{aligned} \tag{21}$$

where Ξ is the normalization constant. The equation for the dressed (measurable) vorticity is

$$\begin{aligned} g_{\mathrm{d}}(\omega) \propto \int \mathrm{d}\vec{r}\, \frac{f(\omega)}{\omega + \beta_{\mathrm{Rossby}} r + (\beta/\gamma)\psi(\vec{r})}&\left[1 - \frac{(1-q)\gamma}{f(\omega)}\left(\omega + \beta_{\mathrm{Rossby}} r + \frac{\beta}{\gamma}\psi(\vec{r})\right)^2\right]^{q/(1-q)} \\ \times \Bigg(&\left[1 + 2\frac{(1-q)\gamma\omega_{\mathrm{m}}}{f(\omega) - (1-q)\gamma(\omega + \beta_{\mathrm{Rossby}} r + (\beta/\gamma)\psi(\vec{r}))^2}\left(\omega + \beta_{\mathrm{Rossby}} r + \frac{\beta}{\gamma}\psi(\vec{r})\right)\right]^{1/(1-q)} \\ &- \left[1 - 2\frac{(1-q)\gamma\omega_{\mathrm{m}}}{f(\omega) - (1-q)\gamma(\omega + \beta_{\mathrm{Rossby}} r + (\beta/\gamma)\psi(\vec{r}))^2}\left(\omega + \beta_{\mathrm{Rossby}} r + \frac{\beta}{\gamma}\psi(\vec{r})\right)\right]^{1/(1-q)}\Bigg). \end{aligned} \tag{22}$$

Thus if we first solve Eq. (13) for the stream function, then we can use ψ in Eq. (22) to compute the PDF of the dressed vorticity. In Section 6 we compare the vorticity PDFs predicted for the extensive and nonextensive cases with the experimental observations.

4. Experimental setup

The experimental system is shown in Fig. 1 and described in the original report on our measurements on turbulence in a rapidly rotating annulus with asymmetric forcing [10]. The annulus has an inner radius $r_{\mathrm{i}} = 10.8$ cm, outer radius $r_{\mathrm{o}} = 43.2$ cm, a sloping bottom, and a flat transparent lid. The bottom depth varies from 17.1 cm at the inner

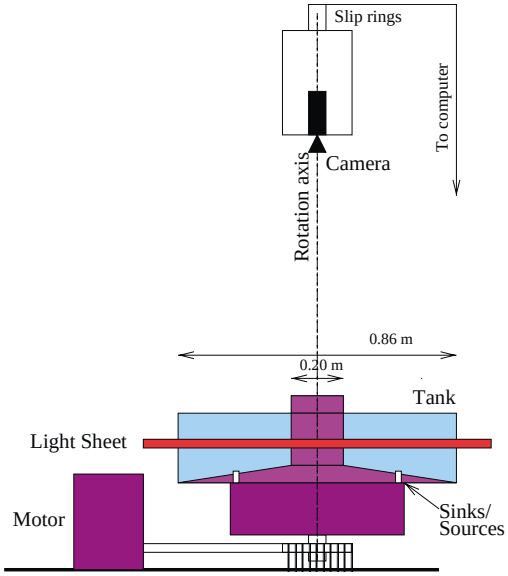

Fig. 1. Schematic representation of the experimental apparatus. The tank rotates up to 3 Hz and water circulates through holes in the bottom. In a rotating frame, the camera obtains images of passive scalar particles (polystyrene spheres, 100–200 μm diameter) suspended in the flow.

radius to 20.3 cm at the outer radius, with a mean height $h_0 = 18.7$ cm and a bottom slope $\eta = -0.1$. For the data analyzed in this paper, the rotation frequency of the annulus is $\Omega/2\pi = 2.5$ Hz.

Water is continuously pumped through the tank in a closed circuit via a ring of 120 circular holes located at the bottom of the tank at the mean radius of the annulus, $r_f = 27$ cm. To avoid direct forcing of a zonal flow, the pumping holes are arranged in two semi-circles: one semi-circle of the pumping holes contains sources and the opposite semi-circle contains sinks; thus zero net vorticity is injected. Each hole has a diameter of 2.5 mm and the total pumping rate is 150 cm^3/s.

The water is seeded with neutrally buoyant plastic particles of size of 150–200 μm. Light emitting diodes produce a 3 cm thick horizontal sheet of light that illuminates the annulus at mid-depth. The particles suspended in the water are imaged with a camera located 2 m above the annulus; the camera rotates with the tank. Particle image velocimetry (PIV) is used to obtain the full two-dimensional velocity field.

The flow can be characterized by three dimensionless numbers, the Reynolds, Rossby, and Ekman numbers. The characteristic velocity $U = 7$ cm/s and length $L = 20$ cm yield a Reynolds number $UL/\nu = 7000$; thus the flow is turbulent. The Rossby number (ratio of inertial to Coriolis force) is $\omega_{\mathrm{rms}}/2\Omega = 0.05$, which indicates that the Coriolis force is dominant, as is the case for planetary flows on large length scales, where Rossby numbers are typically in the range 0.05–0.2. Finally, the small Ekman number, $\nu/2L^2\Omega = 5 \times 10^{-4}$, indicates that dissipation in the bulk is small. The Ekman time from dissipation in the boundary layers is 25 s, much longer than the typical vortex turnover time, 2 s. The dimensionless numbers indicate that the flow is quasi-geostrophic; previous studies of turbulence in the annulus have indeed confirmed the strong two-dimensionality of the flow [9].

5. Results

In this section we compare the solution for the stream function in Eq. (13) with the measurements of the azimuthally averaged vorticity (preliminary results were published in Ref. [33]). Using that stream function we compare the PDF

of the measured vorticity with the expressions derived using the extensive and nonextensive formalisms, Eqs. (15) and (22), respectively.

5.1. Qualitative flow features

In the previous work, we demonstrated that our forcing configuration with no net vorticity injection yields a quasi-geostrophic flow with three jets alternating in their azimuthal direction [10]. Although the net vorticity injected is zero, the β plane (sloping bottom) acts as vorticity selector: cyclonic (anticyclonic) structures cannot move outward (inward) because their motion outward (inward) would trigger a Rossby wave, thus restoring them to their original position. Positive (negative) potential vorticity is carried to the inner (outer) region of the annulus. Within the inner and outer regions the potential vorticity is well mixed. Further, we found the potential vorticity profile was independent of forcing and rotation rate [10].

As seen in Fig. 2, large anticyclones and cyclones appear intermittently. These structures drift in the direction opposite to the annulus rotation. The coherent vortices are created and decay in the region where the inlet–outlet semi-circles meet. A large coherent vortex is typically dissipated after traveling 180° in the azimuthal direction.

5.2. Stream function solution and the vorticity profile

Eq. (13) involves two parameters: the β-plane coefficient, $\beta_{\text{Rossby}} \equiv 2\eta\Omega/h_0 = 0.196\,\text{rad/s cm}$ (see Section 4), and the unknown parameter β/γ, which is determined by fitting the predicted vorticity profile to the experimental data. One boundary condition needed to solve Eq. (13) is given by the condition that the azimuthally averaged vorticity is zero at $r = r_f$ because one-half of the forcing ring contains sources and the other half sinks; thus $\int \omega|_{r=r_f}\,d\theta = 0$. The other boundary condition is that the total circulation should be conserved, $\oint \vec{u}\,d\vec{l} = 0 = \int \omega r\,dr\,d\theta$ (see Eq. (A.3)).

The observed radial profile for the vorticity is compared with the best fit profile in Fig. 3. The predicted vorticity profile exhibits the qualitative features of the measured vorticity, and the locations of the predicted maxima and minima are in reasonable quantitative agreement with experiment. Note that value of the fit parameter is $\beta/\gamma =$

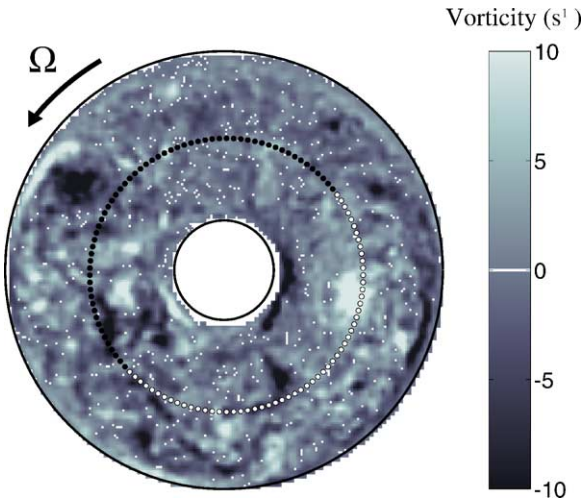

Fig. 2. The measured vorticity field from an experiment with rotation rate 2.5 Hz and pumping rate 550 cm^3/s contains strong cyclones (bright) and anticyclones (dark). The forcing holes are arranged in semi-circles of 60 sources (white dots) and 60 sinks (black dots).

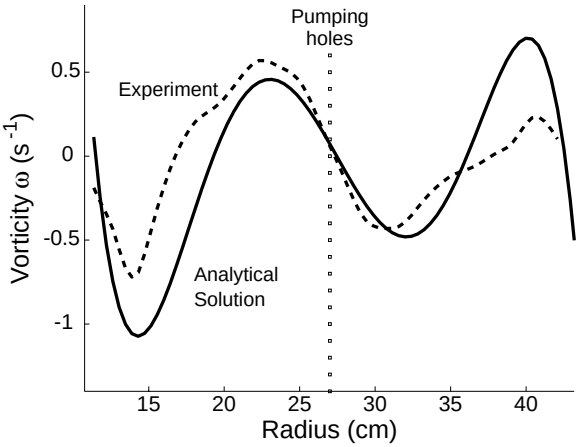

Fig. 3. A comparison of the measured and the predicted radial profile for the vorticity. The theoretical curve is given by a least-squares fit to the solution of Eq. (13), which yields a value for the only adjustable parameter, $\beta/\gamma = -0.169$.

-0.169. One reason for the difference between the model and the measurements is that the real fluid is viscous while the model assumes an inviscid fluid. The viscosity is dominant near the walls and is responsible for the generation of vorticity that is injected into the mean flow, an effect not captured by the theory.

5.3. *Vorticity PDF*

The extensive and nonextensive formalisms yield the same equation for the stream function, but the two approaches predict different PDFs for the vorticity, Eqs. (15) and (22), respectively. The nonextensive model involves the

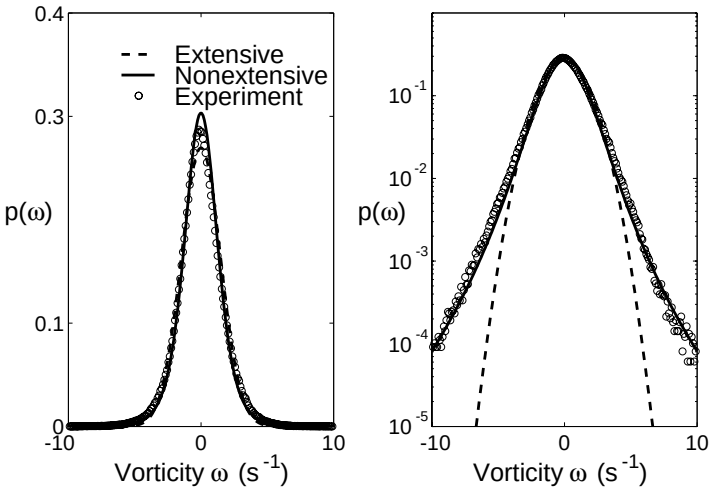

Fig. 4. Comparison of the measured vorticity probability distribution function with the predictions of the extensive and nonextensive energy–enstrophy models, Eqs. (15) and (22), respectively. The linear plot on the left facilitates a comparison of the peaks of the PDF, and the log plot on the right facilitates a comparison of the tails of the distribution. The theoretical curves are least-squares fits that minimize $|(p_{\text{experiment}}(\omega) - p_{\text{model}}(\omega))/p_{\text{model}}(\omega)|^2$ over 96 velocity fields. Using $\beta/\gamma = -0.169$ from the fit to the vorticity radial profile (Fig. 1) leaves two fit parameters, ω_{m} (0.7 ± 0.2) and γ (0.25 ± 0.03) for the extensive model, and three parameters for the nonextensive model, ω_{m} (0.7 ± 0.2), γ (0.15 ± 0.01) and the nonextensive parameter, q (1.9 ± 0.2). The uncertainties are the standard deviations of the fits to 96 different velocity fields.

parameter q, which is absent from the extensive theory; the tails of the vorticity distribution are broad for $q > 1$ and narrow for $q < 1$ (see Appendices B.2 and B.3). The predictions from the two models are compared to the measurements in Fig. 4. Using the value of $\beta/\gamma = -0.169$ obtained in the previous subsection, we have a single fit parameter, ω_m, for the extensive model and two fit parameters, ω_m and q, for the nonextensive model (see Fig. 4). The nonextensive model describes the data over the entire range of vorticity, including both the peak and the broad tails of the distribution. In contrast, the extensive model fails to capture the broad tails of the distribution. The broad tails arise from the large coherent cyclones and anticyclones.

6. Discussion

Assuming conservation of energy and enstrophy, we have constructed models of two-dimensional inviscid flows using both extensive and nonextensive entropy. The two models yield the same prediction for the radial dependence of the azimuthally averaged vorticity. The model involves a single fit parameter and provides good agreement with the observations (Fig. 3). The extensive and nonextensive models yield different predictions for the vorticity PDF. The nonextensive model accurately describes the entire PDF, including the broad tails of the distribution (Fig. 4), which are not described by the extensive model. The value obtained for the nonextensive parameter is $q = 1.9 \pm 0.2$. Previous experiments with our system configured with an inner ring of sources and an outer ring of sinks produced a strong turbulent anticyclonic circulation. An analysis of structure function data from that experiment yielded $q = 1.32 \pm 0.03$ [15]. Experiments in our laboratory on turbulent Couette–Taylor flow were analyzed by Beck et al. [13], who found that the velocity increment structure function data yielded $q = 1.17$ for nearby spatial points. As expected, q decreased to unity for large separations between the points. Measurements by La Porta et al. [34] of the acceleration of passive scalar particles in a strong turbulent shear flow have been analyzed by Beck [16], who obtained $q = 1.49$.

Acknowledgements

The authors thank Christian Beck, Jori Ruppert-Felsot, Eran Sharon and Sung Joon Moon for helpful discussions. This research was supported by the Office of Naval Research.

Appendix A. Extensive energy–enstrophy model

A.1. Equation of stream function

We find the probability of the microscopic vorticity in the equilibrium state, $p(\sigma, \vec{r})$, by maximizing the entropy, where the microscopic vorticity is assumed to fluctuate continuously within the range $\pm\omega_m$.

$$-\nabla^2\psi = \frac{\int_{\omega(\vec{r})-\omega_m}^{\omega(\vec{r})+\omega_m} d\sigma\, \sigma\, e^{-\gamma(\sigma+\beta_{Rossby} r+(\beta/\gamma)\psi(\vec{r}))^2}}{\int_{\omega(\vec{r})-\omega_m}^{\omega(\vec{r})+\omega_m} d\sigma\, e^{-\gamma(\sigma+\beta_{Rossby} r+(\beta/\gamma)\psi(\vec{r}))^2}}$$
$$= \frac{\int_{-\omega_m}^{\omega_m} W\, e^{-\gamma W^2}\, dW}{\int_{-\omega_m}^{\omega_m} e^{-\gamma W^2}\, dW} - \left(\beta_{Rossby} r + \frac{\beta}{\gamma}\psi(\vec{r})\right) \frac{\int_{-\omega_m}^{\omega_m} e^{-\gamma W^2}\, dW}{\int_{-\omega_m}^{\omega_m} e^{-\gamma W^2}\, dW} = -\left[\beta_{Rossby} r + \frac{\beta}{\gamma}\psi(\vec{r})\right], \qquad (A.1)$$

where $W \equiv \sigma - \omega(\vec{r})$. The above equation yields

$$\frac{\partial^2\psi}{\partial r^2}+\frac{1}{r}\frac{\partial\psi}{\partial r}+\frac{1}{r^2}\frac{\partial^2\psi}{\partial\theta^2}-\frac{\beta}{\gamma}\psi=\beta_{\text{Rossby}}r. \tag{A.2}$$

We apply two boundary conditions. First, total circulation is conserved in the annulus, yielding the boundary condition

$$\int\omega\,\mathrm{d}\vec{r}=-\int\frac{1}{r}\frac{\partial}{\partial r}\left[r\frac{\partial\psi}{\partial r}\right]r\,\mathrm{d}r=-r_{\text{i}}\left.\frac{\partial\psi}{\partial r}\right|_{r=r_{\text{i}}}+r_{\text{o}}\left.\frac{\partial\psi}{\partial r}\right|_{r=r_{\text{o}}}=0. \tag{A.3}$$

The second boundary condition is the mean vorticity over the forcing ring is zero,

$$\int\omega|_{r=r_{\text{f}}}\,\mathrm{d}\theta=0. \tag{A.4}$$

The pumping holes consist of a semi-circle of sources and a semi-circle of sinks. We determine β/γ by fitting the solution for ψ with the experimental data, as shown in Fig. 1.

A.2. Probability density function of vorticity

The PDF of microscopic velocity can be expressed from the Boltzmann distribution

$$g(\sigma)=\int p(\sigma,\vec{r})\,\mathrm{d}\vec{r}=\sqrt{\frac{\gamma}{\pi}}\int\mathrm{d}\vec{r}\,\mathrm{e}^{-\gamma(\sigma+\beta_{\text{Rossby}}r+(\beta/\gamma)\psi(\vec{r}))^2}=\sqrt{\frac{\gamma}{\pi}}\int\mathrm{d}\vec{r}\,\mathrm{e}^{-\gamma(\sigma+\beta_{\text{Rossby}}r+(\beta/\gamma)\psi(\vec{r}))^2}. \tag{A.5}$$

It is impossible to measure the microscopic vorticity directly. Miller et al. suggested a dressed vorticity density corollary $g_{\text{d}}(\omega)$, which is a measurable vorticity on any finite scale [29],

$$\begin{aligned}g_{\text{d}}(\omega)&\equiv\frac{1}{V}\int\mathrm{d}\vec{r}\,\delta(\omega'(\vec{r})-\omega)=\frac{1}{V}\int\mathrm{d}\vec{r}\langle\omega'(\vec{r})|\omega\rangle=\frac{1}{V}\int\mathrm{d}\vec{r}\int\mathrm{d}\sigma'\langle\omega'(\vec{r})|\sigma'\rangle\langle\sigma'|\omega\rangle\\&=\frac{\gamma}{\pi}\int\mathrm{d}\vec{r}\int\mathrm{d}\sigma'\,\mathrm{e}^{-\gamma(\sigma'-\omega)^2+\gamma(\sigma'-\omega'(\vec{r}))^2}\propto\int\mathrm{d}\vec{r}'\,\mathrm{e}^{-\gamma(\omega^2-\omega'(\vec{r})^2)}\int_{\omega(\vec{r})-\omega_{\text{m}}}^{\omega(\vec{r})+\omega_{\text{m}}}\mathrm{d}\sigma'\,\mathrm{e}^{-2\gamma\sigma'(\omega'(\vec{r})-\omega)}\\&\propto\int\mathrm{d}\vec{r}\frac{1}{\omega-\omega'(\vec{r})}\,\mathrm{e}^{-\gamma(\omega-\omega(\vec{r}))^2}\sinh\left(2\gamma\omega_{\text{m}}(\omega-\omega'(\vec{r}))\right),\end{aligned} \tag{A.6}$$

where $\omega'(\vec{r})$ is defined as $\beta_{\text{Rossby}}r+(\beta/\gamma)\psi(\vec{r})$ and $\langle\sigma|\omega\rangle$ is the probability of microscopic quantity, σ, at the given macroscopic quantity ω. The original work of Miller uses $\omega_{\text{m}}\to\infty$, meaning that the microsopic vorticity makes $g_{\text{d}}(\omega)$ diverge. Therefore, we assume a lower and higher cutoff of microscopic vorticity, ω_{m}.

Appendix B. Nonextensive energy–enstrophy model

B.1. Equation of stream function

By maximizing the nonextensive entropy in Eq. (3), we can derive an equation for the stream function,

$$\begin{aligned}-\nabla^2\psi&=\frac{\int_{\omega(\vec{r})-\omega_{\text{m}}}^{\omega(\vec{r})+\omega_{\text{m}}}\mathrm{d}\sigma\,\sigma\,\mathrm{e}_q^{-\gamma(\sigma+\beta_{\text{Rossby}}r+(\beta/\gamma)\psi(\vec{r}))^2}}{\int_{\omega(\vec{r})-\omega_{\text{m}}}^{\omega(\vec{r})+\omega_{\text{m}}}\mathrm{d}\sigma\,\mathrm{e}_q^{-\gamma(\sigma+\beta_{\text{Rossby}}r+(\beta/\gamma)\psi(\vec{r}))^2}}=-\left(\beta_{\text{Rossby}}r+\frac{\beta}{\gamma}\psi(\vec{r})\right)\frac{\int_{-\omega_{\text{m}}}^{\omega_{\text{m}}}\mathrm{d}W\,\mathrm{e}_q^{-\gamma W^2}}{\int_{-\omega_{\text{m}}}^{\omega_{\text{m}}}\mathrm{d}W\,\mathrm{e}_q^{-\gamma W^2}}\\&=-\left(\beta_{\text{Rossby}}r+\frac{\beta}{\gamma}\psi(\vec{r})\right),\end{aligned} \tag{B.1}$$

where $e_q^x \equiv (1+(1-q)x)^{1/(1-q)}$. These results are valid for both $q<1$ and $q>1$. Note that this nonextensive analysis yields the same equation for the stream function as the extensive analysis.

B.2. PDF of vorticity when $q>1$

If we know the functional form of the probability of the microscopic vorticity, $p(\sigma,\vec{r})$, we can calculate the normalization factor as follows:

$$\int p^q \,\mathrm{d}\sigma = \frac{1}{Z^q}\int_{-\omega_\mathrm{m}}^{\omega_\mathrm{m}} \left(1-\frac{(1-q)\gamma}{f(\omega)}W^2\right)^{q/(1-q)} \mathrm{d}W$$
$$= \frac{1}{Z^q}\int_{-\omega_\mathrm{m}}^{\omega_\mathrm{m}} (1-y^2)^{q/(1-q)}\,\mathrm{d}y\sqrt{\frac{f(\omega)}{(q-1)\gamma}} = \Xi^{-1} f(\omega)^{1/2}, \tag{B.2}$$

where $f(\omega)=1+(1-q)\gamma\omega^2$ and $y=\sqrt{(q-1)\gamma/f(\omega)}W$. The PDF of vorticity is given as

$$g(\sigma) = \int \mathrm{d}\vec{r}\frac{p^q}{\int p^q\,\mathrm{d}\sigma} = \int \mathrm{d}\vec{r}\,\frac{\{1-((1-q)\gamma/f(\omega))(\sigma+\beta_\mathrm{Rossby}r+(\beta/\gamma)\psi(\vec{r}))^2\}^{q/(1-q)}}{\Xi^{-1}f(\omega)^{1/2}}$$
$$= \Xi\int \mathrm{d}\vec{r}\left(1-\frac{(1-q)\gamma}{f(\omega)}\left(\sigma+\beta_\mathrm{Rossby}r+\frac{\beta}{\gamma}\psi(\vec{r})\right)^2\right)^{q/(1-q)} f(\omega)^{-1/2}. \tag{B.3}$$

The dressed vorticity is given by

$$g_\mathrm{d}(\omega) = \int \mathrm{d}^2r\int \mathrm{d}\sigma'\,\frac{\{1+((q-1)\gamma/f(\omega))(\sigma'-\omega)^2\}^{q/(1-q)} f(\omega)^{1/2}}{\{1+((q-1)\gamma/f(\omega'))(\sigma'-\omega'(\vec{r}))^2\}^{q/(1-q)} f(\omega'(\vec{r}))^{1/2}}. \tag{B.4}$$

Consider the region $\Sigma^<$, which satisfies $|((q-1)\gamma/f(\omega))(\sigma-\omega)^2|<1$. We have $|\omega-\omega_\mathrm{m}/2|>\sqrt{1/(2\gamma(q-1)\omega_\mathrm{m})}$ and $|\omega-\omega_\mathrm{m}/2|<\sqrt{1/(2\gamma(q-1))-\omega_\mathrm{m}^2/4}$ in $\Sigma^<$, and the inequalities are reversed in the region $\Sigma^>$. With these conditions we can approximate Eq. (B.4) as

$$g_\mathrm{d}^{\Sigma^<} = \int_{\Sigma^<}\mathrm{d}\vec{r}\int \mathrm{d}\sigma'\left(1-\frac{(1-q)\gamma}{f(\omega)}(\sigma'-\omega)^2+\frac{(1-q)\gamma}{f(\omega'(\vec{r}))}(\sigma'-\omega'(\vec{r}))^2+\cdots\right)^{q/(1-q)}, \tag{B.5}$$

$$g_\mathrm{d}^{\Sigma^<} \approx \int_{\Sigma^<}\mathrm{d}\vec{r}\int_{\omega(\vec{r})-\omega_\mathrm{m}}^{\omega(\vec{r})+\omega_\mathrm{m}}\mathrm{d}\sigma'\left[1-\frac{(1-q)\gamma}{f(\omega)}(\omega^2-\omega'(\vec{r})^2)-\frac{(1-q)\gamma}{f(\omega)}2\sigma'(\omega'(\vec{r})-\omega)\right]^{q/(1-q)}$$
$$\propto \int_{\Sigma^<}\mathrm{d}\vec{r}\frac{f(\omega)}{\omega-\omega'(\vec{r})}\left[1-\frac{(1-q)\gamma}{f(\omega)}(\omega-\omega'(\vec{r}))^2\right]^{q/(1-q)}$$
$$\times\left(\left[1+2\frac{(1-q)\gamma\omega_\mathrm{m}}{f(\omega)-(1-q)\gamma(\omega-\omega'(\vec{r}))^2}(\omega-\omega'(\vec{r}))\right]^{1/(1-q)}\right.$$
$$\left.-\left[1-2\frac{(1-q)\gamma\omega_\mathrm{m}}{f(\omega)-(1-q)\gamma(\omega-\omega'(\vec{r}))^2}(\omega-\omega'(\vec{r}))\right]^{1/(1-q)}\right). \tag{B.6}$$

We use the approximation that $f(\omega)\sim f(\omega')$ because ω is close to ω' for the dressed vorticity. The limit of $q\to 1$ approaches the result in the extensive case. If $\gamma(q-1)$ and $\omega_\mathrm{m}^2/4$ are very small, $g_\mathrm{d}^{\Sigma^>}$ is negligible compared to $g_\mathrm{d}^{\Sigma^<}$. From experimental data, we found that $\gamma(q-1)\sim 0.14$ and $\omega_\mathrm{m}^2/4\sim 0.12$. Therefore, $g_\mathrm{d}\approx\sigma_\mathrm{d}^{\Sigma^<}$.

B.3. PDF of vorticity when $q < 1$

The PDF of vorticity is obtained as

$$\int p^q \,\mathrm{d}\sigma = \frac{1}{Z^q}\int \left(1 - \frac{(1-q)\gamma}{f(\omega)}W^2\right)^{q/(1-q)} \mathrm{d}W = \frac{1}{Z^q}\sqrt{\frac{f(\omega)}{(1-q)\gamma}}\left(\frac{1}{2}, \frac{1}{1-q}\right) = \Xi^{-1} f(\omega)^{1/2} \tag{B.7}$$

by using $\int_0^1 (1-x^2)^{\mu-1}\,\mathrm{d}x = (1/2)B(1/2,\mu)$. We can assume that W is confined to the range $(-1 < \sqrt{(1-q)\gamma/f(\omega)}W < 1)$ because values outside this range result in nonphysical interpretations such as negative partition function.

$$\begin{aligned} g(\sigma) &= \int \mathrm{d}\vec{r}\,\frac{p^q}{\int p^q\,\mathrm{d}\sigma} = \int \mathrm{d}\vec{r}\frac{\{1-((1-q)\gamma/f(\omega))(\sigma-\omega)^2\}^{q/(1-q)}}{f(\omega)^{1/2}\Xi^{-1}} \\ &= \Xi\int \mathrm{d}\vec{r}\left(1-\frac{(1-q)\gamma}{f(\omega)}(\sigma-\omega)^2\right)^{q/(1-q)} f(\omega)^{-1/2}, \end{aligned} \tag{B.8}$$

where $f(\omega) = 1 + (1-q)\gamma\omega^2$. The dressed velocity distribution is given by

$$\begin{aligned} g_{\mathrm{d}}(\omega) &= \int \mathrm{d}\vec{r}\int \mathrm{d}\sigma' \frac{\{1-((1-q)\gamma/f(\omega))(\sigma'-\omega)^2\}^{q/(1-q)} f(\omega)^{-1/2}}{\{1-((1-q)\gamma/f(\omega'(\vec{r})))(\sigma'-\omega'(\vec{r}))^2\}^{q/(1-q)} f(\omega'(\vec{r}))^{-1/2}} \\ &\propto \int \mathrm{d}\vec{r}\frac{f(\omega)}{(\omega-\omega')}\left[1-\frac{(1-q)\gamma}{f(\omega)}(\omega-\omega')^2\right]^{q/(1-q)} \\ &\quad\times\left(\left[1+2\frac{(1-q)\gamma\omega_{\mathrm{m}}}{f(\omega)-(1-q)\gamma(\omega-\omega')^2}(\omega-\omega')\right]^{1/(1-q)}\right. \\ &\quad\left.-\left[1-2\frac{(1-q)\gamma\omega_{\mathrm{m}}}{f(\omega)-(1-q)\gamma(\omega-\omega')^2}(\omega-\omega')\right]^{1/(1-q)}\right). \end{aligned} \tag{B.9}$$

As before, we use the approximation $f(\omega) \sim f(\omega')$. In the limit $q \to 1$, we obtain the extensive case. With the approximation

$$g_{\mathrm{d}}(\omega) \approx \left[1-\frac{(1-q)\gamma}{f(\omega)}(\omega-\omega')^2\right]^{q/(1-q)},$$

we find that the fourth and higher moments of vorticity diverge for $q \geq 2$ because $\int_0^\infty x^{n-1}(1+x^2)^{-q/(q-1)}\mathrm{d}x$ converges when $q > n/(n-2)$.

References

[1] P. Tabeling, Phys. Rep. 362 (2002) 1.
[2] L. Onsager, Nuovo Cimento Suppl. 6 (1949) 279.
[3] R.H. Kraichnan, Phys. Fluids 10 (1967) 1417.
[4] R.H. Kraichnan, in: E. Jen (Ed.), 1989 Lectures in Complex Systems, Addison-Wesley, Redwood City, 1989, p. 271.
[5] R.H. Kraichnan, S. Chen, Physica D 37 (1989) 160–172.
[6] J. Miller, Phys. Rev. Lett. 65 (1990) 2137.
[7] P.T. Landsberg, J. Statist. Phys. 35 (1984) 159.
[8] C.N. Baroud, B.B. Plapp, Z.S. She, H.L. Swinney, Phys. Rev. Lett. 88 (2002) 114501.
[9] C.N. Baroud, B.B. Plapp, H.L. Swinney, Z.S. She, Phys. Fluids 15 (2003) 2091.

[10] J. Aubert, S. Jung, H.L. Swinney, Geophys. Res. Lett. 29 (2002) 1876.
[11] C. Tsallis, J. Statist. Phys. 52 (1988) 479;
C. Tsallis, Physica D, 10.1016/j.physd.2004.01.006, this volume.
[12] http://tsallis.cat.cbpf.br/biblio.htm.
[13] C. Beck, G.S. Lewis, H.L. Swinney, Phys. Rev. E 63 (2001) 035303.
[14] C. Beck, Phys. Lett. A 287 (2001) 240.
[15] C.N. Baroud, H.L. Swinney, Physica D 184 (2003) 21.
[16] C. Beck, Phys. Rev. Lett. 87 (2001) 180601.
[17] X.P. Huang, C.F. Driscoll, Phys. Rev. Lett. 72 (1994) 2187.
[18] B.M. Boghosian, Phys. Rev. E 53 (1996) 4754.
[19] J. Pedlosky, Geophysical Fluid Dynamics, Springer, New York, 1987.
[20] G. Holloway, Ann. Rev. Fluid Mech. 18 (1986) 91.
[21] M. Lesieur, Turbulence in Fluids, Kluwer Academic Publishers, Dordrecht, 1997.
[22] R.H. Kraichnan, D. Montgomery, Rep. Prog. Phys. 43 (1980) 547.
[23] D. Montgomery, L. Turner, G. Vahala, Phys. Fluids 21 (1978) 57.
[24] W.H. Matthaeus, D. Montgomery, Ann. NY Acad. Sci. 357 (1980) 203.
[25] M.R. Brown, J. Plasma Phys. 57 (1997) 203.
[26] C. Tsallis, Braz. J. Phys. 29 (1999) 1.
[27] C. Tsallis, R.S. Mendes, A.R. Plastino, Physica A 261 (1998) 534.
[28] D. Lynden-Bell, Month. Not. R. Astron. Soc. 136 (1967) 101.
[29] J. Miller, P.B. Weichman, M.C. Cross, Phys. Rev. A 45 (1992) 2328.
[30] R. Robert, J. Sommèria, J. Fluid Mech. 229 (1991) 291–310.
[31] C.E. Leith, Phys. Fluids 27 (1984) 1388.
[32] H. Brands, P.H. Chavanis, R. Pasmanter, J. Sommeria, Phys. Fluids 11 (1999) 3465.
[33] S. Jung, B.D. Storey, J. Aubert, H.L. Swinney, in: A.J. Smits (Eds.), Reynolds Number Scaling in Turbulent Flow, Kluwer Academic Publishers, Dordrecht, 2003, pp. 137–140.
[34] A. La Porta, G.A. Voth, A.M. Crawford, J. Alexander, E. Bodenschatz, Nature 409 (2001) 1017.